Available online at www.sciencedirect.com
ScienceDirect
Surface & Coatings Technology 201 (2007) 6460–6464
SURFACE & COATINGS TECHNOLOGY
www.elsevier.com/locate/surfcoat

# Atmospheric plasma deposition of glass coatings on aluminum

A. Ladwig [a,c], S. Babayan [b], M. Smith [a], M. Hester [a], W. Highland [a], R. Koch [a], R. Hicks [c,*]

[a] National Nuclear Security Administration's Kansas City Plant, Kansas City, Missouri, United States
[b] Surfx Technologies LLC, 3617 Hayden Avenue, Culver City, California, United States
[c] Department of Chemical Engineering, University of California, Los Angeles, California, United States

Received 12 August 2006; accepted in revised form 20 December 2006
Available online 29 December 2006

**Abstract**

The deposition and properties of glass coatings on aluminum was investigated using atmospheric pressure plasma-enhanced chemical vapor deposition. The plasma, generated with radio frequency power at 27.12 MHz, was fed helium, oxygen and two types of silicon precursors, hexamethyldisilazane and tetraethylorthosilicate. After deposition, the coatings were analyzed for composition, adhesion and dielectric strength. X-ray photoelectron spectroscopy revealed that the glass coatings contained approximately 25% silicon, 50% oxygen and 25% carbon. Scratch tests indicated that the coatings were strongly adherent to the substrates. The glass coatings achieved DC dielectric strengths in between 50 and 250 V for a thickness range of 0.5 to 1.3 μm. The maximum breakdown voltage measured was 400 V. Scanning electron microscopy revealed that breakdown occurred at cracks and other defects in the coatings. These defects appeared to form around areas of surface roughness and contamination.
© 2007 Elsevier B.V. All rights reserved.

*Keywords:* Glass; Aluminum; HMDSN; PECVD

## 1. Introduction

Treatments that enhance the performance of metal substrates, such as increased dielectric strength and wear resistance, have become increasingly important as applications continue to require highly functional parts. Although techniques such as powder coating are readily available for the treatment of larger-sized metal substrates [1], these macroscopic techniques are not suitable for parts in the millimeter or below range as they are not conformal and are generally applied too thick. Well-established thin film coating techniques, such as physical vapor deposition and chemical vapor deposition, are available for parts below a micron (i.e. MEMS) [2]. However, these techniques can be complex and overly-sophisticated for a production environment focusing on parts with dimensions between 25 μm and 2.5 mm.

Plasma-enhanced chemical vapor deposition (PECVD) is a low-temperature processing method that is readily adapted to complex mechanical parts. However, a drawback of this technique is that it is carried out inside a vacuum chamber that is costly and requires significant maintenance [3]. Furthermore, vacuum processes cannot accommodate pressure-sensitive components without the risk of damage. In an effort to eliminate some of these drawbacks, alternative coating methods have been development, including atmospheric pressure glow discharge (APGD) [4,5] and the sol–gel technique [6,7].

In this report, we investigate another atmospheric pressure PECVD alternative, as developed by Babayan et al. [8], specifically for the deposition of glass (silicon dioxide) coatings on aluminum substrates. It is found that the coatings are strongly adherent with good dielectric strength but are subject to cracking when surface imperfections or particle contamination are present.

## 2. Experimental methods

The apparatus consisted of a Surfx Technologies LLC, A-250D deposition system. This system was operated at 100 W of radio frequency (RF) power at 27.12 MHz. The deposition tool,

* Corresponding author. Tel.: +1 310 806 6865; fax: +1 305 206 4107.
*E-mail address:* rhicks@ucla.edu (R. Hicks).

0257-8972/$ - see front matter © 2007 Elsevier B.V. All rights reserved.
doi:10.1016/j.surfcoat.2006.12.018

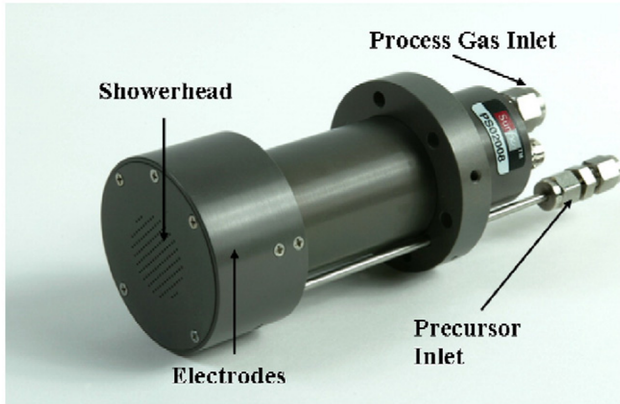


Fig. 1. Atmospheric plasma deposition tool.

possessing a 5.1 $cm^2$ showerhead is shown in Fig. 1. A schematic of its operation is shown in Fig. 2.

The plasma was formed by feeding the process gases, helium and oxygen, into the system upstream of the electrodes at flow rates of 30.0 L/min and 450.0 mL/min, respectively. Two types of silicon precursors were investigated: hexamethyldisilazane (HMDSN) and tetraethylorthosilicate (TEOS). These volatile precursors were introduced into the plasma, downstream of the electrodes, by bubbling helium through the liquid at 0.4 and 1.0 L/min for HMDSN and TEOS, respectively. The silicon precursors were kept in temperature controlled baths at 21 °C. Samples were processed at deposition times ranging from 5.0 to 20.0 min at a distance of 5.0 cm downstream of the showerhead. The silicon dioxide was deposited onto the center of 2.5″ × 3.0″ aluminum samples. All samples were ultrasonically cleaned in trichloroethylene, treated for 1.0 min with an oxygen plasma and then heated to 250 °C prior to deposition. Unless indicated otherwise below, the glass coatings were prepared with the HMDSN precursor.

X-ray photoelectron spectroscopy was used to analyze the composition of the coatings. The instrument was a KRATOS Analytical Axis Ultra DLD spectrometer with a focused monochromator (Al $K_\alpha$ radiation at 1486.6 eV) and Ar+ sputtering capability. The composition of the coatings was also analyzed by infrared spectroscopy using a Bio-Rad FTS-40A with a DTGS detector. Scanning electron microscopy (SEM) was used to evaluate the surface morphology of the coatings.

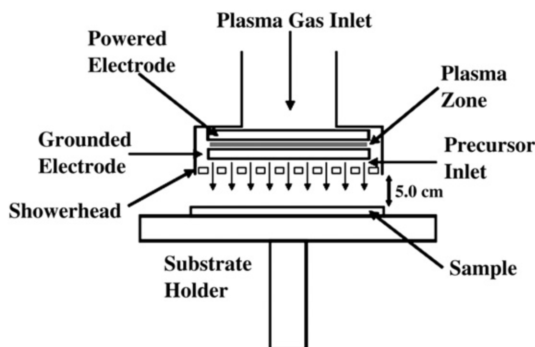


Fig. 2. Schematic of atmospheric plasma deposition tool.

Table 1
Composition and binding energies of glass coatings grown with $O_2$/He plasma and HMDSN

| Thickness | C1s | | Si 2p | | O1s | |
|---|---|---|---|---|---|---|
| | Binding energy (eV) | at. % | Binding energy (eV) | at. % | Binding energy (eV) | at. % |
| 0.5 μm | 285.1 | 16.0 | 104.6 | 22.6 | 533.6 | 54.9 |
| | 286.3 | 2.1 | 102.0 | 2.1 | | |
| | 287.8 | 1.0 | | | | |
| 1.3 μm | 285.0 | 24.7 | 104.5 | 19.4 | 533.9 | 47.9 |
| | 286.3 | 3.2 | 101.9 | 1.8 | | |
| | 287.8 | 1.6 | | | | |

Thickness data were gathered by ellipsometry, using silicon substrates instead of aluminum, but prepared under identical growth conditions. The adhesion of the glass to the Al substrates was evaluated by a standard tape pull test, ASTM D3359. A 3.0 $cm^2$ area of the film was cross-hatched, after which Permacel #99 tape was firmly applied and then removed. This adhesion test provides quantitative results only if adhesion fails; therefore, an optical microscope was utilized to determine if the adhesion failed, with special attention given to the corners of the cross-hatched squares.

Breakdown voltages were measured on the samples using an Associated Research Hypot III 3665 per ASTM D3755. The voltage was applied at a ramp rate of 500 VDC/s through a 1/4″

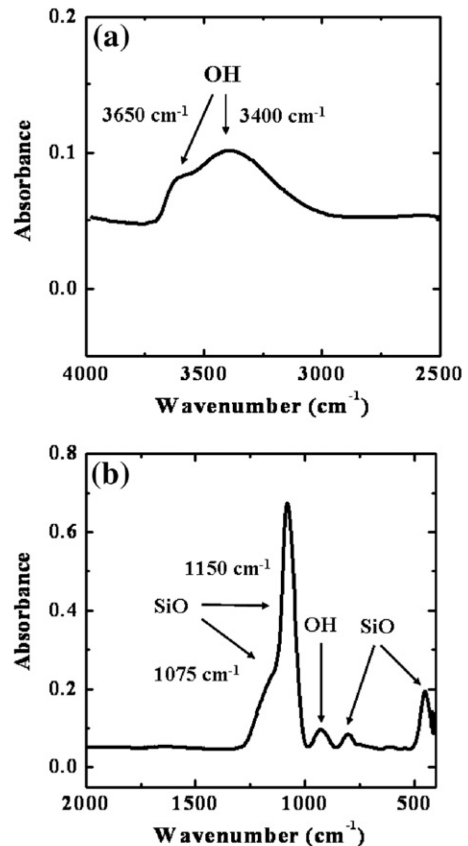


Fig. 3. Infrared absorbance spectra of glass coating grown with $O_2$/He plasma and HMDSN.

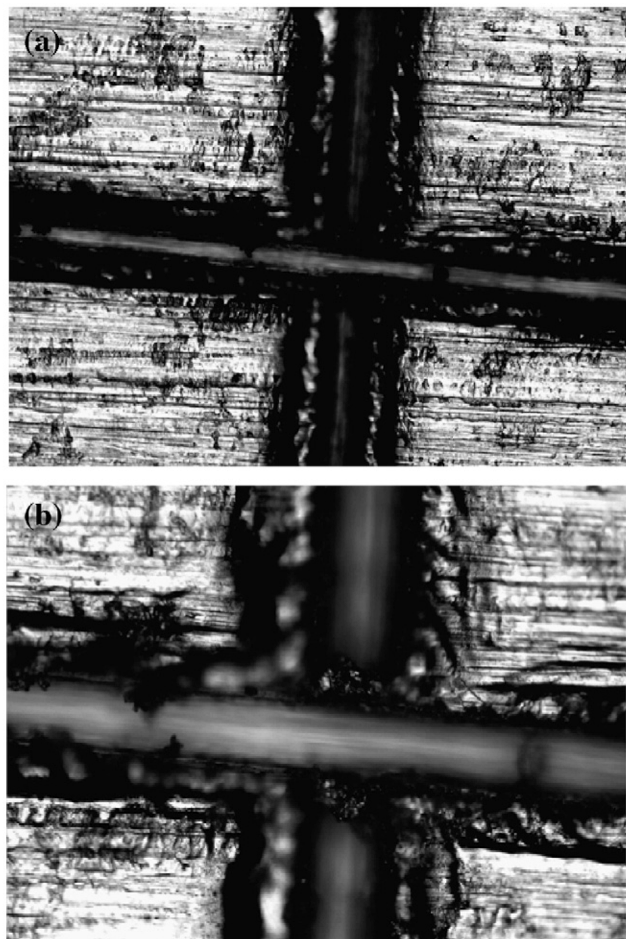


Fig. 4. Images of cross-hatch adhesion test of glass coatings, 10X (a) and 20X (b).

diameter electrode. Five locations on each sample were tested: four around the perimeter of the deposition area and one in the center. The dielectric strength reported is an average of these five measurements. Results obtained from this test included dielectric strength as well as breakdown. The dielectric strength was recorded for samples that were able to withstand the applied voltage during the ramp period plus a dwell period of 1.0 s once the desired voltage level had been reached. Breakdown was measured by applying a voltage large enough to cause failure, which was detected as a sudden increase in current above 7.5 mA. This phenomenon may also be accompanied by a visual rupture of the film.

## 3. Results and discussion

Shown in Table 1 are the binding energies and atomic percentages of the silicon, oxygen and carbon present in the glass coatings prepared using HMDSN. The nitrogen content was determined to be negligible and was omitted. The coatings were comprised of 21 to 25 at.% silicon, 48 to 55 at.% oxygen and 19 to 29 at.% carbon. The presence of carbon in the film is believed to be due to incomplete decomposition of the HMDSN precursor.

The C 1*s* peak was deconvoluted into three peaks with the two smallest peaks at approximately 286.3 eV and 287.8 eV representing carbonyl or carbonate-like bonding. The highest intensity peak at $285.0 \pm 0.1$ eV was due to C–Si bonding which is as expected for methyl ligands present in partially decomposed HMDSN. After deconvolution, a primary Si 2*p* shoulder at approximately $102.0 \pm 0.1$ eV was found which may be associated with silicon atoms that still contain Si–C linkages, while the main peak was observed at $104.5 \pm 0.1$ eV due to $SiO_2$.

In Fig. 3 infrared absorbance spectra are presented of an HMDSN film deposited at 250 °C for 13 min. Peaks of interest include those from the asymmetric stretching, bending and rocking modes of siloxane bridges at 1150, 1075, 800 and 450 $cm^{-1}$ and those for the stretching modes of hydroxyl groups at 3650 and 3400 $cm^{-1}$. In the literature, the presence of hydroxyl groups has been used as an indication of film porosity [9]. In particular, the ratio of the siloxane shoulder at 1150 $cm^{-1}$ to the primary peak at 1075 $cm^{-1}$ can give an estimate of the degree of porosity. Porosity can be indicative of a weaker, less insulating coating. The absorbance spectra of the glass coatings shown here are consistent with a low degree of porosity.

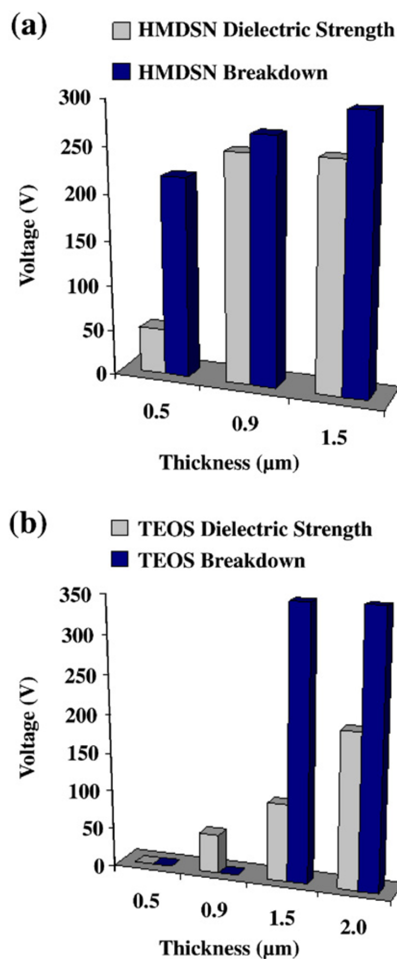


Fig. 5. Dielectric strength and breakdown of glass coatings grown using HMDSN (a) and TEOS (b).

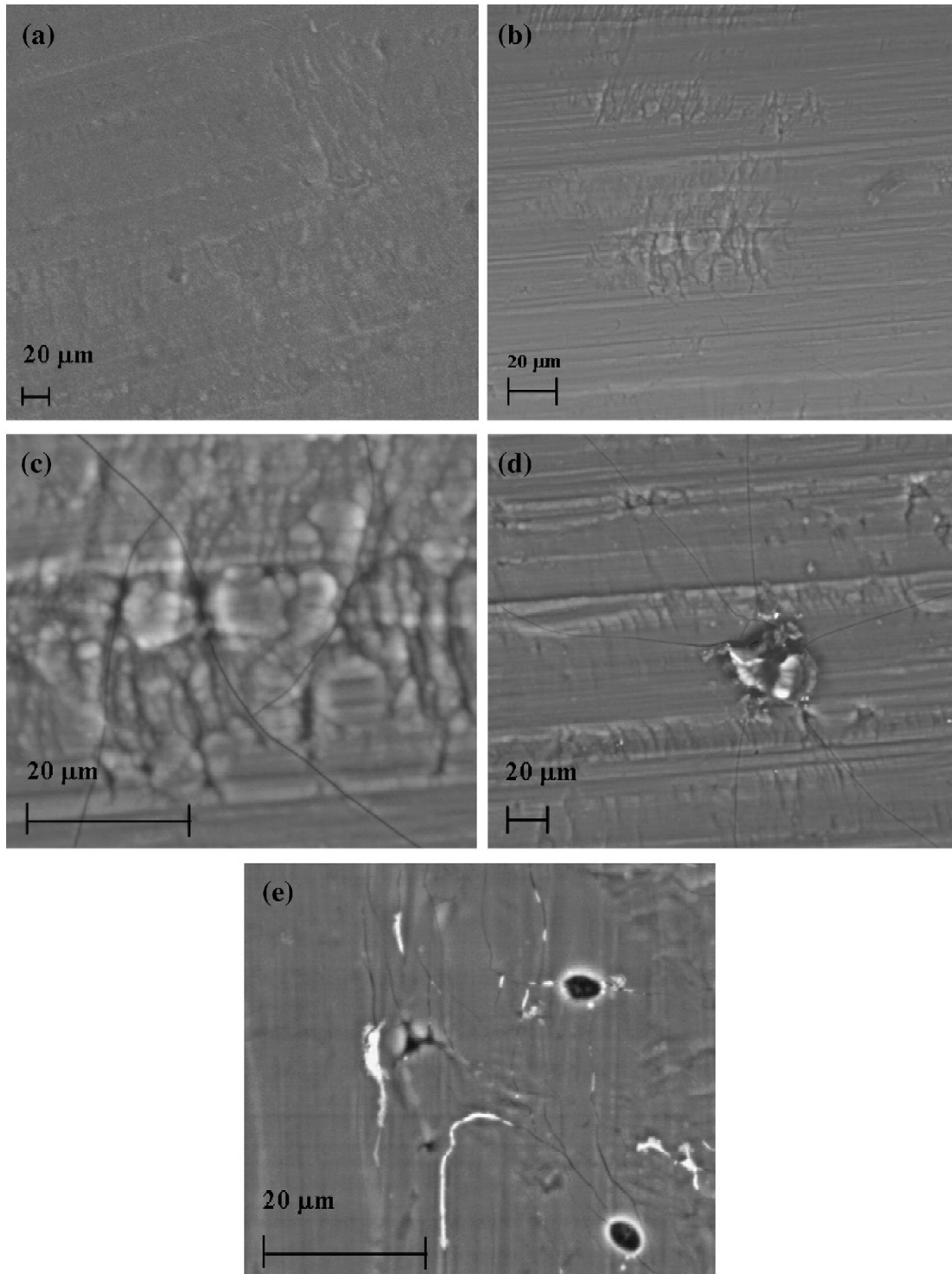


Fig. 6. Scanning electron microscopy images of glass coatings on aluminum: a) bare aluminum (300×); b) aluminum and glass surface (300×); c) aluminum and glass surface (1000×); d) particulate contamination (454×), and e) coating after dielectric breakdown (1000×).

Adhesion tests revealed that the glass coatings are strongly adherent to the aluminum. If adhesive failure were to occur between the coating and the Al substrate, it would do so at the intersection of the cross-hatch squares. Optical images of the cross-hatch pattern in the glass coatings are presented in Fig. 4. No failure in the adhesion can be discerned.

Dielectric strength data for the glass samples are presented in Fig. 5. Five points across the 1″ diameter of each film was tested and averaged. Dielectric strength refers to the amount of voltage the samples were able to consistently withstand without failing, while breakdown represents the voltage at which the samples failed when tested to failure, producing a sudden jump in current. For both HMDSN and TEOS coatings, the dielectric strength and breakdown increased as the film thickness increased, with a maximum dielectric strength of 250 V and 200 V observed for HMDSN and TEOS coatings

with a thickness of 0.9 and 2.0 μm, respectively. As expected, the breakdown voltage was consistently higher than the strength measurement. Dielectric breakdown values of glass coatings that have been deposited utilizing well-established methods have been reported to range from $10^6$–$10^7$ V/cm [10,11] depending on the thickness. The HMDSN coatings yielded a maximum breakdown of 300 V ($2.0 \times 10^6$ V/cm), while the maximum for the TEOS coatings was 350 V ($1.75 \times 10^6$ V/cm). It is important to note that TEOS breakdown was not consistent and for many samples was only found in one of the five test locations.

The deposition temperature also has an affect on the dielectric strength. It was observed that for deposition at 100 °C, the glass coatings prepared from TEOS had no detectable dielectric strength or breakdown voltage, whereas the coatings prepared from HMDSN exhibited inconsistent dielectric strength results with a maximum value of 50 V achieved. As previously reported [9], higher process temperatures reduce impurities, such as hydroxyl groups, as these impurities are more volatile and can be desorbed from the coating.

Scanning electron microscopy was performed to examine failure modes of the glass coatings following dielectric strength testing. Shown in Fig. 6 are five micrographs taken at different positions on the film. In Fig. 6a, a bare Al substrate prior to silicon dioxide deposition is shown. Areas of roughness on the Al substrate are observed. Rough regions of the Al substrate, after silicon dioxide deposition, are also observed in Fig. 6b and c. In the latter image, one sees cracks emanating from the rough area. In Fig. 6d, cracks are seen radiating from particulate contamination. Finally, in Fig. 6e, cracks in the glass coatings are evident at pinholes created from DC dielectric breakdown testing. Regions of surface roughness are observed to be in close proximity to the pinholes.

Despite the fact that the substrates were thoroughly cleaned prior to deposition, particulates such as dust appear to have been incorporated into the coating. These particulates as well as rough areas of the metal surface seem to be a source of cracks in the coatings. In addition, they may be sites where breakdown occurs under the applied voltage. It may be that by providing a smoother surface finish and performing the deposition in a clean room environment, one could eliminate the source of cracking the coatings and achieve dielectric strengths that are higher than the 250 V obtained herein.

## 4. Conclusions

Strongly adherent glass coatings have been deposited on aluminum substrates by atmospheric plasma-enhanced chemical vapor deposition at 250 °C using volatile silicon precursors and $O_2$ and He plasma. The coatings were found to be highly adherent to the aluminum substrates. In addition, scanning electron microscopy revealed that rough areas of the substrate and contamination may have adversely affected the dielectric strength, despite observing consistent values of ~250 V.

## Acknowledgement

This work is supported by a Cooperative Research and Development Agreement between the National Nuclear Security Administration's Kansas City Plant and Surfx Technologies LLC.

## References

[1] A.T. Misey, Powder Coatings: Chemistry and Technology, John Wiley and Sons, New York, 1991.
[2] C.T. Leondes, MEMS/NEMS Handbook: Techniques and Applications, vol. 5, Springer, New York, 2006.
[3] A. Schütze, J.Y. Jeong, S.E. Babayan, J. Park, G.S. Selwyn, R.F. Hicks, IEEE Trans. Plasma Sci. 26 (1998) 1685.
[4] L.J. Ward, W.C.E. Schofield, J.P.S. Baydal, A.J. Goodum, P.J. Merlin, Langmuir 19 (2003) 2110.
[5] L.J. Ward, W.C.E. Schofield, J.P.S. Baydal, A.J. Goodum, P.J. Merlin, Chem. Mater. 15 (2003) 1466.
[6] Y. Kaneko, N. Iyi, T. Matsumoto, H. Usami, J. Mater. Res. 20 (2005) 2199.
[7] C. McDonagh, F. Sheridan, T. Butler, B.D. MacCraith, J. Non-Cryst. Solids 194 (1996) 72.
[8] S.E. Babayan, J.Y. Jeong, V. Tu, G.S. Selwyn, R.F. Hicks, Plasma Sources Sci. Technol. 7 (1998) 286.
[9] G.R. Knowling, M. Yajima, S.E. Babayan, M. Moravej, X. Yang, W. Hoffman, R.F. Hicks, Plasma Sources Sci. Technol. 14 (2005) 477.
[10] S. Franssila, Introduction to Microfabrication, Wiley, London, 2004, p. 59.
[11] J.H. Stathis, IBM J. Res. Develop. 46 (2002) 266.